INTERNATIONAL JOURNAL OF PROGRESSIVE RESEARCH IN ENGINEERING MANAGEMENT AND SCIENCE (IJPREMS)
(Int Peer Reviewed Journal)
Vol. 04, Issue 10, October 2024, pp : 618-633
www.ijprems.com
editor@ijprems.com
e-ISSN : 2583-1062
Impact Factor : 7.001

# A NOVEL KSK CONVERTER WITH MACHINE LEARNING RBFNN MPPT FOR PV APPLICATIONS USING MATLAB

**N. Deena Nepolian[1], Dr. Abhisha Mano[2], B. P. Beno Ben[3]**

[1]Assistant Professor, Ece Department Annai Vailankanni College Of Engineering, Pottalkulam Azhagappapuram Post, Kanyakumari District, Tamilnadu, India.

[2]Assistant Professor, Ece Department Dmi Engineering College, Aralvoimozhi Tamil Nadu India.

[3]Assistant Professor, Eee Department John Cox Memorial Csi Institute Of Technology, Medical College, Po, Thiruvananthapuram, Kerala, India.

DOI: https://www.doi.org/10.58257/IJPREMS36293

## ABSTRACT

Power electronic converters are regarded as an indispensable aspect of modern electric power system, owing to their eminence as an optimal power interface and power flow regulator. Hence, the design of an efficient converter is vital to support the wide scale expansion in application of both Electric Vehicles (EVs) and Renewable Energy Sources (RES). Thereby, a novel high gain KSK converter based on interleaved architecture, exhibiting lower voltage stress across switches is proposed in this research work. The suggested converter design is well suited for Photovoltaics (PV) power generation, as it offers higher step-up gain with lower input current ripples. Moreover, the mathematical analysis and modelling of suggested KSK converter with its different operational modes is also covered in this article. Additionally, to optimize the power generated from the PV system, a Machine Learning (ML) based Radial Basis Function Neural Network (RBFNN) is implemented as Maximum Power Point Tracking (MPPT) technique. Additionally, Internet of Things (IoT) is used for real time monitoring of the PV parameters. The viability of suggested KSK converter is demonstrated through MATLAB simulation and laboratory prototype implementation, while the control of the developed 1000W prototype is entrusted up on FPGA Spartan 6E controller. Consequently, the achieved exceptional 98.6% efficiency of the proposed KSK converter lends credence to its excellence over other published converter topologies.

**Keywords:** PV system, EV, novel KSK converter, RBFNN MPPT

## 1. INTRODUCTION

Electricity being the crux of modern life cannot be overstated as it enables economic development, social progress and environmental sustainability. Its ample supply is indeed imperative to power the modern-day comforts and conveniences of humans. However, the majority of its global production is based on fossil fuels, which are currently in a phase of steady decline. Additionally, its widespread use also poses serious social and environmental impacts, consequently shifting the global energy perspective towards Renewable Energy Sources (RESs), which are comparatively abundant and cleaner in nature with low-to-zero carbon emission. Along with RESs, the swift transition to low-carbon economy is also supported by technologies like Electric Vehicles (EVs), bulk energy storage, smart grid and Hybrid Electric Vehicles (HEVs) [1-3]. The conversion and control of power in all these technologies are accomplished using power electronic devices, which over the decades has undergone tremendous transition due to dynamic technology evolution. Particularly, the PV system, which is a vital RESs that has witnessed an unprecedented growth rate in recent times, requires the support of the power electronic interface as illustrated in Figure 1 to improve its raw output voltage level that is fundamentally lower than the desired utility level. As seen in the Figure, an optimal DC-DC converter design ensures that the Maximum Power Point (MPP) of the solar panels is tracked accurately, resulting in maximum energy output and system efficiency [4, 5].

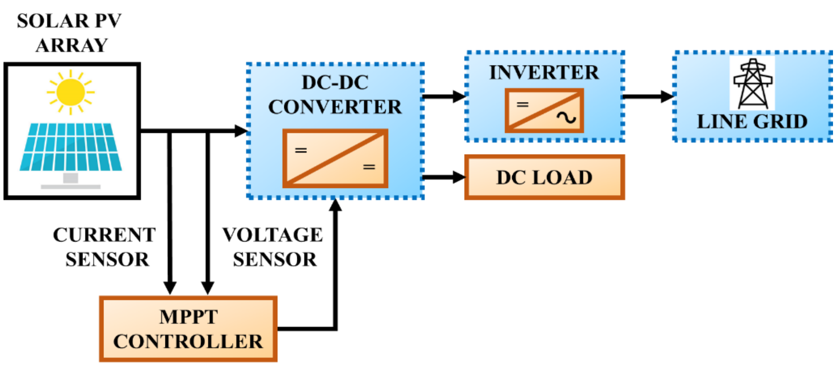


**Figure:** PV system with its power electronic interface

The Boost converter [6] is undeniably the most popular choice as DC-DC converter for PV system applications, since it has a simple topology and infinite voltage boosting capability as per its voltage gain equation. Even so, when used for practical applications, its operation is mostly carried out at an extremely high duty cycle of 0.88. Additionally, it also encounters certain other restrictions in the form of conduction losses, commutation issues, reverse recovery issue and high switching voltage stress. In case of Buck-Boost converter [7], which also has a simple topology, exhibits negative output voltage polarity. Moreover, at high duty cycle like the Boost converter, the Buck-Boost converter also encounters gain limitations due to the voltage drop caused by inductor internal resistance. The Cuk [8] and SEPIC [9] converter can be considered as the offshoots of Buck-Boost converter with additional components in their circuit topologies. Both these converters exhibit continuous input current, where the former is capable of voltage inversion, while the latter is capable of accomplishing high voltage conversion ratio. The property of providing voltage regulation even when the input voltage is lower or higher than the voltage output, also differentiates these converters from the Buck-Boost converter. But, at the same time, the low frequency voltage ripple exhibited by Cuk converter and the high-frequency current ripple exhibited by SEPIC converter leaves them unsuited for MPPT operations [10]. The Luo converter [11] excels over SEPIC and Cuk converter on account of its high efficiency, simple control, wide input voltage range, low voltage stress and high output voltage gain. The generation of high-frequency noise, however, dampers the effectiveness of Luo converter as an optimal DC-DC converter topology. Meanwhile, it is possible to subdue these drawbacks faced by conventional converters using the Interleaved converter topology [12-14] as it offers improved power handling capability, higher efficiency, better transient response, reduced component stress in addition to minimum input and output ripples. Thereby, in this work, a novel KSK converter based on interleaved topology with wide input voltage range and suitability for a variety of applications is proposed.

An effective MPPT technique plays an instrumental role in improving the converter efficiency by always ensuring the operation of PV panels at MPP to accomplish highest possible power output. The Perturb and Observation (P&O) [15] is a simple MPPT technique, where the PV panel operating point is perturbed by varying either the current or voltage and studying the consequent variation in output power. It also compares the power output at each perturbed point to the power output at the previous point and adjusts the operating point in the direction of higher power output. However, the efficiency of this technique is limited due to its slow response and its tendency to oscillate around MPP. In case of Incremental Conductance (IC) [16], the MPP is reached by comparing the instantaneous conductance of the PV system to its incremental conductance. This MPPT technique also encounters certain limitations in the form of measurement errors and high noise sensitivity. The Fractional Open Circuit Voltage (FOCV) [17] is another conventional MPPT technique, which is established on the relationship between the open-circuit voltage (OCV) of PV module and its MPP. The accuracy of FOCV is affected by the changes in operating conditions, making them unsuited for non-ideal conditions. The Fuzzy Logic Control (FLC) MPPT [18] is a type of Artificial Intelligence (AI) based MPPT that works by using a set of rules to determine the direction and magnitude of the perturbation to the PV system operating point. The advantage of FLC MPPT lies in its ability to handle imprecise input data and non-uniform operating conditions. However, this technique is more complex to implement than other MPPT algorithms, as it requires more computational resources, which in turn tends to be a disadvantage in certain applications. The Artificial Neural Network (ANN) [19] MPPT is a type of ML based MPPT, which determines MPP by training a neural network model on a set of historical data that includes the voltage, current, and power output of PV system under distinct operating conditions. This technique is an efficient and accurate MPPT approach with great adaptability to operating condition changes, but on the downside, it requires large amount of training data and involves a complex training process. Thus, in this work, RBFNN MPPT technique is used for optimizing the working of KSK converter as it is capable of providing a more accurate and efficient MPPT solution with faster training and simpler implementation than both ANN and FLC MPPT techniques.

A novel KSK converter designed based on interleaved architecture is presented in this work to efficiently transfer the DC power generated by the PV panel to the load or the grid by providing the necessary voltage regulation. The KSK converter offers enhanced efficiency, power density in addition to reduced current ripples and voltage stress. Moreover, the KSK converter with the assistance of RBFNN MPPT enables the PV system to operate at MPP, where the power output is optimized. Furthermore, the predictive maintenance of the entire system is ensured using real-time IoT based parameter monitoring.

## 2. PROPOSED SYSTEM DESCRIPTION

The modern power generation sector stipulates for an optimal DC-DC converter design to facilitate the wide-scale implementation of PV systems owing to its critical role in improving the overall efficiency, flexibility, and scalability of the system. Hence, in this work, a robust KSK converter design based on interleaved architecture is presented. As seen in Figure 1, the voltage and current output from the PV system is provided to KSK converter as input. The presented KSK converter is designed by interleaving the SEPIC converter topology with Super Lift Luo converter. Thus, resulting in the development of an optimal DC-DC converter design with excellent power handling capability, efficiency, transient response and minimum component stress. Moreover, the aspect of distribution of input and output current among the individual converters of the interleaved architecture, facilitates the reduction of current ripples in the KSK converter. Additionally, the property of minimum component stress of the KSK converter leads to significant reduction in power losses.

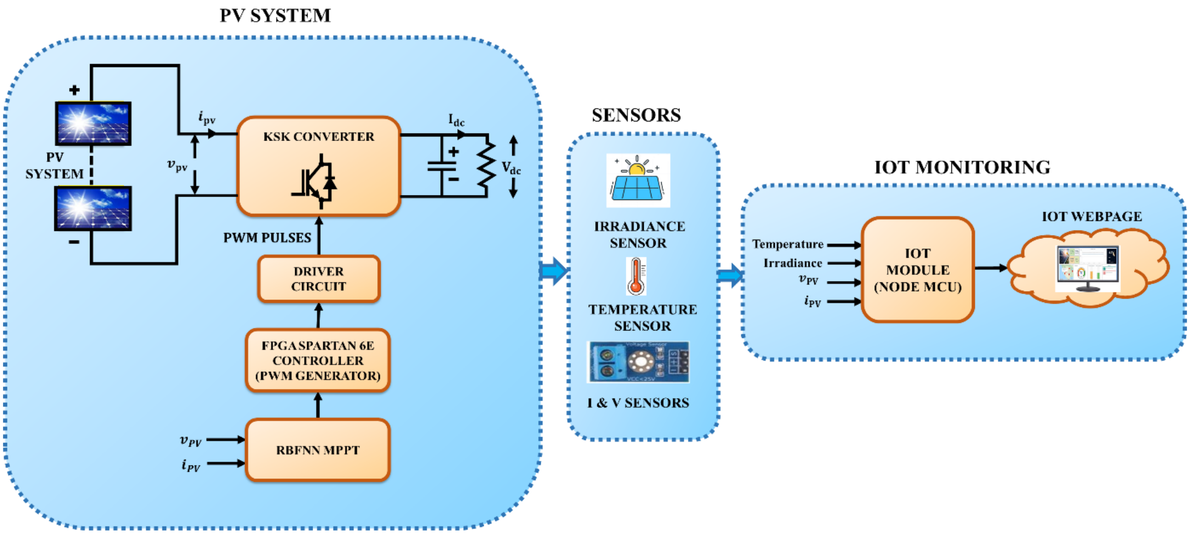


**Figure 2:** The proposed IoT based PV system with KSK converter and RBFNN MPPT

The KSK converter duty cycle signal is generated by RBFNN MPPT, which in turn ensures the maximum power extraction from PV system. This process is accomplished by the RBFNN MPPT by taking the current values of $V_{PV}$, $I_{PV}$, and temperature as inputs and determine the duty cycle required for maximum power extraction from the PV panel as output. The predicted duty cycle is then fed to the KSK converter in the form of control signals by the PWM generator. The parameters such are temperature, irradiance, PV voltage and PV current are sensed using sensors. These sensed real time data are collected by Node MCU before being transmitted to the cloud.

## 3. PROPOSED SYSTEM MODELLING

### A) PV SYSTEM MODELLING

When sunlight hits the PV array, the PV cells in the panels absorb the energy and release electrons that subsequently flow through the connected circuitry and generate a Direct Current (DC) electricity, which is expressed as,

$$I_{PV} = N_p \left[ I_{ph} - I_o \left\{ e^{q(V_{PV}+R_S I_{PV})/AkTN_s} - 1 \right\} - \frac{V_{PV}+R_S I_{PV}}{N_S R_p} \right] \quad (1)$$

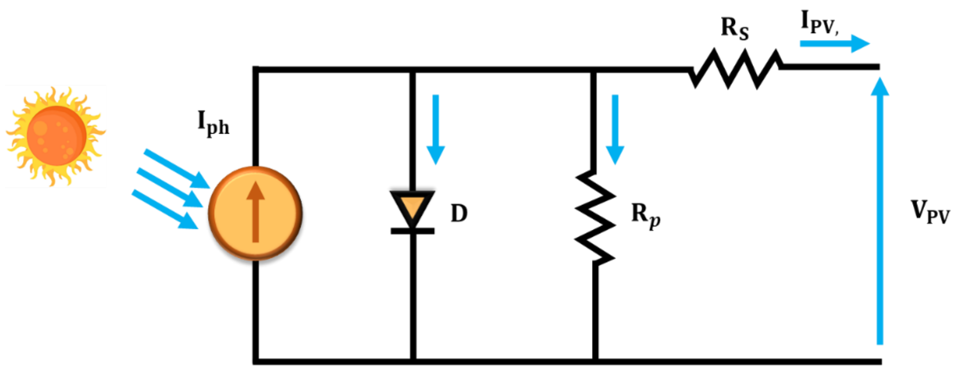


**Figure:** Single diode model-based representation of PV cell

The fundamental principle behind the working of PV cell is studied utilizing a single diode model that is presented in Figure 3. This model is used to design and optimize PV cells for maximum efficiency, and to predict the PV array performance under different environmental conditions. In equation (1), the current generated by the absorption of sunlight in the semiconductor material of the PV cell is represented as $I_{ph}$, the current that flows through the p-n junction of the PV cell is represented as $I_o$, the term $R_p$ represents the resistance that allows the flow of small amount of current around the p-n junction and the term $R_s$ represents the resistance that occurs due to the inherent resistance of the semiconductor material. Moreover, the terms $q, T, k$ and $A$ are the electric charge $(1.6021 \times 10^{-19} C)$, temperature in Kelvin, Boltzmann's constant $(1.3805 \times 10^{-23}\ J/K)$ and dimensionless junction material factor respectively.

**B) KSK CONVERTER MODELLING**

A novel KSK converter is introduced in this work to provide a more enhanced and efficient power conversion solution to PV system. The presented KSK converter as seen in Figure 4, is obtained by interleaving SEPIC with Super Lift Luo converter. The former is capable of improving the PV panel voltage with galvanic isolation between the input and output, while the latter is a variant of the Luo Converter that uses a coupled inductor to achieve a high step-up voltage. Moreover, the highly efficient Super Lift Luo converter is also known for its low input current ripple. Thus, by interleaving both these converters, the overall efficiency and power density of the power supply system is further improved. Here, the high step-up voltage of the Super Lift Luo converter complements the voltage conversion capability of SEPIC converter. Furthermore, the interleaving technique distributes the input and output currents among the individual converters, which reduces the current ripple and improves the overall efficiency. The four different modes of operation of the proposed KSK converter are presented in Figure 5.

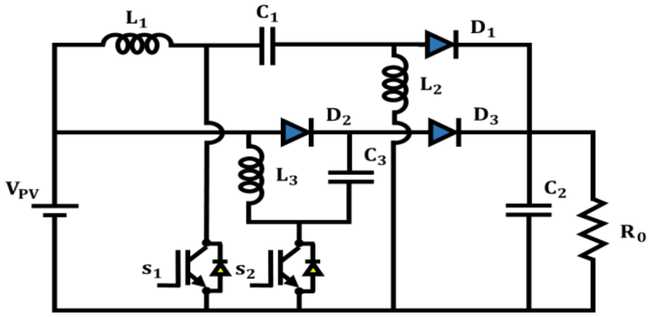


**Figure 4:** The proposed KSK converter topology

**Mode 1$[t_0 - t_1]$:**

During this operational mode, the switch $S_1$ is turned ON and the input voltage from the PV system is applied to the input inductor $L_1$, which in turn leads to the subsequent ramping up of the inductor current. Here, the capacitor $C_1$ transfers its stored charges to inductor $L_2$, resulting in its increased magnetization. The inductor $L_2$ with the increase in its magnetic field, begins to store the dissipated energy from the capacitor. It is also noted that the switch $S_2$ is turned OFF during this mode, resulting in the reverse biased condition of diode $D_2$. Moreover, throughout this mode, the diode $D_1$ is also reverse biased, while the diode $D_3$ is forward biased and conducting. On applying Kirchhoff's Voltage Law (KVL) and Kirchhoff's Current Law (KCL),

$$V_{PV} - L_1 \frac{di_{L_1}}{dt} = 0 \tag{2}$$

$$C_1 \frac{dV_{C_1}}{dt} + i_{L_1} = 0 \tag{3}$$

$$L_2 \frac{di_{L_2}}{dt} - V_{C_1} = 0 \tag{4}$$

$$C_2 \frac{dV_{C_2}}{dt} + \frac{V_{C_2}}{R_o} = 0 \tag{5}$$

$$V_{PV} + V_{C_3} - L_3 \frac{di_{L_3}}{dt} = V_{C_2} = V_o \tag{6}$$

$$C_3 \frac{dV_{C_3}}{dt} + i_{L_3} = 0 \tag{7}$$

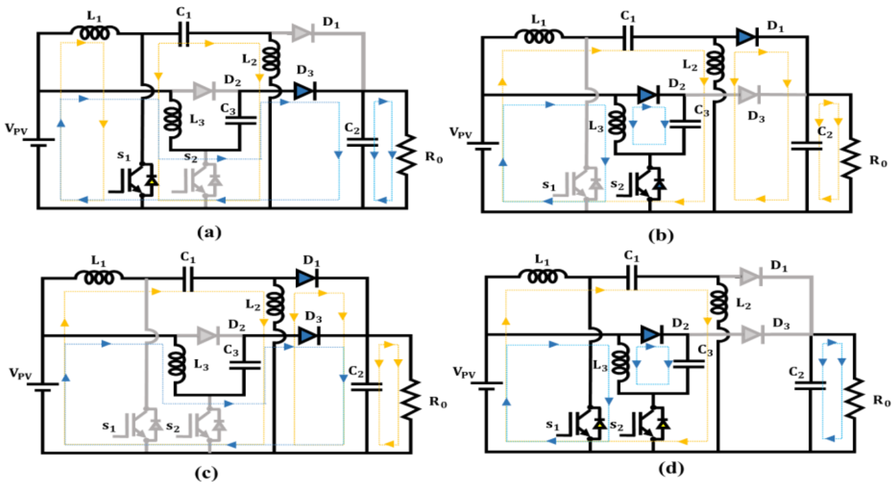


**Figure 5:** Various operational modes of KSK converter

**Mode 2$[t_1 - t_2]$:**

The Mode 2 is the opposite of Mode 1, since the switch $S_1$ is turned OFF and the switch $S_2$ is turned ON during this mode. Moreover, the diodes $D_1$ and $D_2$ are conducting, while the diode $D_3$ is non-conducting. The inductors $L_1$ $and$ $L_2$ are discharging, while the capacitor $C_1$ is charging in this mode. Additionally, the inductor $L_3$ and capacitor $C_3$ are also in charging state and both attain a steady voltage level that is equivalent to that of the input PV voltage.

$$V_{PV} = L_1 \frac{di_{L_1}}{dt} + V_{C_1} + V_{C_2} \quad (8)$$

$$L_2 \frac{di_{L_2}}{dt} + V_{C_1} = 0 \quad (9)$$

$$C_1 \frac{dV_{C_1}}{dt} - i_{L_1} = 0 \quad (10)$$

$$C_2 \frac{dV_{C_2}}{dt} - i_{L_1} - i_{L_2} + \frac{V_{C_2}}{R_o} = 0 \quad (11)$$

$$L_3 \frac{di_{L_3}}{dt} = V_{PV} \quad (12)$$

$$C_3 \frac{dV_{C_3}}{dt} = V_{PV} \quad (13)$$

**Table 1:** Switching state of KSK converter

| Switches $S_1, S_2$ | Diodes $D_1, D_2, D_3$ | Inductors | | | Capacitors | |
|---|---|---|---|---|---|---|
| | | $L_1$ | $L_2$ | $L_3$ | $C_1$ | $C_3$ |
| 1,0 | 0,0,1 | ↑ | ↑ | ↓ | ↓ | ↓ |
| 0,1 | 1,1,0 | ↓ | ↓ | ↑ | ↑ | ↑ |
| 0,0 | 1,0,1 | ↓ | ↓ | ↓ | ↑ | ↓ |
| 1,1 | 0,1,0 | ↑ | ↑ | ↑ | ↓ | ↑ |

$\downarrow -discharging, \uparrow -charging$

**Mode 3$[t_2 - t_3]$:**

In this mode, both the switches are turned OFF, while the diodes $D_1$ and $D_3$ are conducting. The inductor $L_1, L_2$ $and$ $L_3$ are all in discharging mode and the capacitor $C_3$ is also in discharging mode. The components that in the state of storing charges in this mode are capacitors $C_1$ $and$ $C_2$. The charging and discharging states of different components of the converter is given in Table 1.

**Mode 4$[t_3 - t_4]$:**

In this mode, both the switches are turned ON, while the diodes $D_1$ and $D_3$ are non-conducting owing to their reverse biased nature. Unlike mode 3, the inductors are all in charging state along with capacitor $C_3$. Moreover, the magnetic field across the inductors ramps up, leading to the increase in inductor current. On the other hand, the capacitors $C_1$ $and$ $C_2$ discharges and dissipates its stored energy in this mode. The expression for ripple current across inductor $L_1$ is given as,

$$\Delta i_{L_1} = \frac{V_{PV} DT}{L_1} = \frac{V_{PV} D}{L_1 f} \quad (14)$$

Where, the terms $D, T$ $and$ $f$ represents the duty ratio, time period and switching frequency respectively. The expression for ripple current across inductor $L_3$ is given as,

$$\Delta i_{L_3} = \frac{V_o - 2V_{PV}}{L_3}(1-K)T = \frac{V_o - 2V_{PV}}{L_3}\frac{(1-K)}{f} \quad (15)$$

The expression for output ripple voltage is given as,

$$\Delta V_o = \frac{I_o(1-D)T}{C_2} = \frac{1-D}{fC_2}\left(\frac{V_o}{R_o}\right) \quad (16)$$

**Voltage Gain**

The converter voltage gain, which in general is defined as the ratio of the converter output voltage to its input voltage, represents the amount by which the input voltage is multiplied or divided to achieve the desired output voltage. It is a vital parameter that poses a significant impact over the operation of PV system, as it determines the efficiency, power transfer capability, and voltage regulation of the converter.

$$V_{PV} D + (V_{PV} - V_o)(1-D) = 0 \quad (17)$$

The KSK converter voltage gain is estimated as,

$$M = \frac{V_O}{V_{PV}} = \frac{2-D}{1-D} \quad (18)$$

**Semiconductor Components Voltage Stress Analysis**

The analysis of voltage stress of every components plays an instrumental role in ensuring the reliable and efficient operation of the KSK converter. The term voltage stress refers to the maximum voltage that a component experiences during the operation of the converter. Here, the capacitor voltage values are estimated as,

$$V_{C_1} = V_{C_3} = \frac{V_o}{2-D} \quad (19)$$

$$V_{C_2} = V_o \quad (20)$$

The voltage stress of both the IGBT switches is estimated as,

$$V_{S_1} = V_{S_2} = \frac{V_o}{2-D} \quad (21)$$

The voltage stress of the diodes is estimated as,

$$V_{D_1} = \frac{1}{1-D} V_o \quad (22)$$

$$V_{D_2} = V_{D_3} = \frac{1}{2-D} V_o \quad (23)$$

On studying the above equations, it is concluded that the estimated voltage stress on the KSK converter components is lesser than $V_o$. Thus, by achieving lower voltage stress across the components, there is a considerable decrease in power losses, resulting in improved overall KSK converter efficiency.

**Design Considerations**

The value of the inductors is given as,

$$L_1 = L_2 = \frac{V_{PV(min)}}{\Delta L_{L_1} \times f} \quad (24)$$

Where, the term $V_{PV(min)}$ refers to the minimum input voltage.

$$L_3 = \frac{V_o - 2V_{PV}}{\Delta L_{L_1}} \left(\frac{1-D}{f}\right) \quad (25)$$

The value of capacitors is given as,

$$C_1 = C_3 = \frac{I_O \times D}{C_1 \times f} \quad (26)$$

$$C_2 = \frac{(1-D)V_o}{\Delta V_o f R_o} \quad (27)$$

The proposed KSK converter, while maintaining the high efficiency, also allows for a wide range of input and output voltages. Moreover, with lower voltage stress across the components, the lifespan of the components is potentially extended along with improving the converter safety by overcoming the risk of electric arcing and insulation breakdown.

**C) RBFNN MPPT MODELLING**

The RBFNN is a type of neural network, named after the Radial Basis Function (RBF), which is a mathematical function used to transform the input data into a higher dimensional space. The RBFNN is chosen as MPPT approach in this work as it has several advantages over other types of neural networks, such as its ability to approximate non-linear functions and its faster convergence rate. It is also less sensitive to the choice of the initial weights and biases, which makes it easier to train. In the hidden layer, each neuron represents an RBF, which is a Gaussian function centred on a particular data point in the input space. The output layer is a linear combination of the hidden layer neurons, which produces the final output of the network. The RBFNN, when implemented as MPPT techniques, takes PV voltage ($V_{PV}$), PV current ($I_{PV}$) and irradiance ($Ir$) as inputs as seen in Figure. The following equations are used for achieving the different layers of RBFNN,

$$M^y = \begin{bmatrix} I_{yPV} \\ V_{yPV} \\ Ir_y \end{bmatrix} \quad (28)$$

$$\varphi = \begin{pmatrix} \varphi_1^1 & \varphi_2^1 & \varphi_x^1 \\ \varphi_1^2 & \varphi_2^2 & \varphi_x^2 \\ \varphi_1^n & \varphi_2^n & \varphi_x^n \end{pmatrix}, \ [\varphi_k(k = 1,2, \dots, x)] \quad (29)$$

$$N^y = D_y, (y = 1,2,3, \dots n) \quad (30)$$

Where, the terms $M, \varphi$ $and$ $N$ represents the three-dimensional vector of input layer, hidden layer with $x$ RBFs and output layer respectively. The gaussian function used is expressed as,

$$\varphi_k(M^y) = exp\left(\frac{\|M^y - C_k\|^2}{r^2}\right) \quad (33)$$

Where, the term $C_k$ is used to represent the centre of $\varphi_k$ and the scalar quantity is specified using the term $r$.

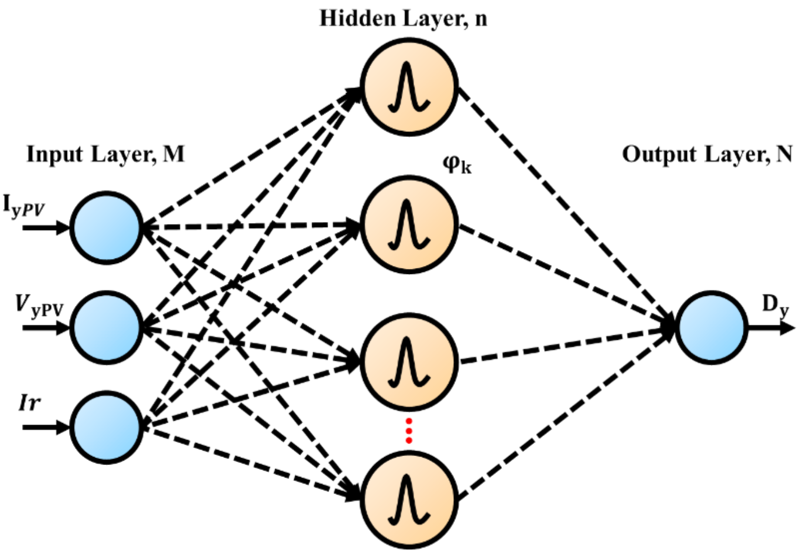


**Figure 7:** Structure of RBFNN MPPT

The expression for the output layer is,

$$N_l^y = \sum_{k=1}^{n} w_{kl}\varphi_k(M^y) + b_k \quad (35)$$

Where, the terms $b_k$ and $w_{kl}$ represents the biases and weighting factors respectively. While training RBFNN for MPPT operation, initially data regarding PV system is collected, following which these data are pre-processed by normalizing the input and output parameters to a range of 0 to 1. Consequently, the data are divided in to training, validation and testing sets. The RBFNN training is accomplished using the training set, while the validation set is used to adjust the RBFNN parameters, such as hidden neurons count and the spread parameter. The testing set is adopted to evaluate the RBFNN performance. Finally, when implemented, the RBFNN in accordance to the given input, generates the duty cycle of KSK converter as output.

### D) PV PARAMETER MONITORING USING IOT

Real-time IoT-based parameter monitoring of the proposed PV system, comprising KSK converter and RBFNN MPPT involves the continuous monitoring of various parameters such as temperature, irradiance, $V_{PV}$, and $V_{PV}$. The monitoring is done using an IoT structure that includes Node MCU, MySQL database cloud service, and IoT webpage as illustrated in Figure 8. The Node MCU is a microcontroller board that is equipped with Wi-Fi connectivity, making it an ideal platform for IoT-based applications. It is used to read the values of the various parameters from the PV system, including the PV panel voltage and current, temperature, and irradiance. The Node MCU then sends these values to the MySQL database cloud service. The MySQL database cloud service is used to store the values of the various parameters in a structured manner. It allows for easy retrieval and analysis of the data from anywhere in the world, as long as an internet connection is available.

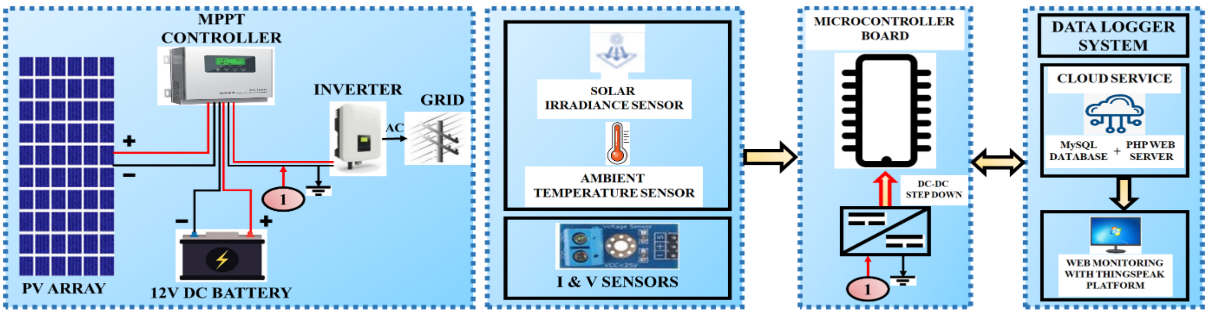


**Figure 8:** IoT based PV parameter monitoring architecture

The MySQL database is accessed through the use of APIs (Application Programming Interfaces), which allow the Node MCU to send data to the database and retrieve data from it. The webpage is used to display the real-time data from the PV system. It is designed using HTML, CSS, and JavaScript, and it communicates with the MySQL database cloud service through APIs. The webpage displays the values of the various parameters in real-time, allowing users to monitor the performance of the PV system. Thus, the IoT-based parameter monitoring system is used to identify any issues with the PV system and take corrective action in real-time. For example, if the temperature of the PV panel exceeds a certain threshold, the system can send an alert to the user, indicating that the cooling system needs to be activated to prevent any damage to the PV panel. Thereby, the real-time IoT-based parameter monitoring of a PV system provides an efficient and effective way to monitor the performance of the PV system. It allows users to identify any issues with the system and take corrective action in real-time, ensuring that the system operates at maximum efficiency.

## 4. RESULTS AND DISCUSSION

In this section, the results obtained using the simulation and laboratory prototype implementation of the KSK converter with cascaded RBFNN MPPT is analysed. The evaluation techniques are employed to evaluate the performance of KSK converter under varying operating scenarios. By simulating the KSK converter in MATLAB platform using the specifications given in Table 1, the vital parameters like efficiency, output voltage/current ripples, stability and transient response are assessed. The prototype implementation analysis further validates and refines the simulated results by considering real-world factors and component limitations. Moreover, simulating the KSK converter before building a physical prototype helps save costs and time as it allows for quick evaluation of multiple design options. Here, the advantages of using MATLAB for simulation includes its user-friendly interface, extensive library of functions, powerful computation capabilities, visualization tools, and community support.

**Table 2:** Simulation parameter specifications

| Parameters | Values |
|---|---|
| **PV system** | |
| Total count of panels | 20 panels, 100W |
| Power | 2000 W |
| $I_{SC}, V_{OC}, V_{SC}$ | 8.33 A,22.6 V,12 V |
| Driver circuit | TLP250 |
| Controller | FPGA Spartan 6E |
| **KSK Converter** | |
| Switching frequency $f_s$ | 10 kHz |
| $L_1, L_2$ | 5.5 mH |
| $L_3$ | 7 mH |
| Output capacitor $C_2$ | 2200 $\mu F$ |
| Input capacitor $C_1, C_3$ | 870$\mu F$ |
| Load | 100 Ω |

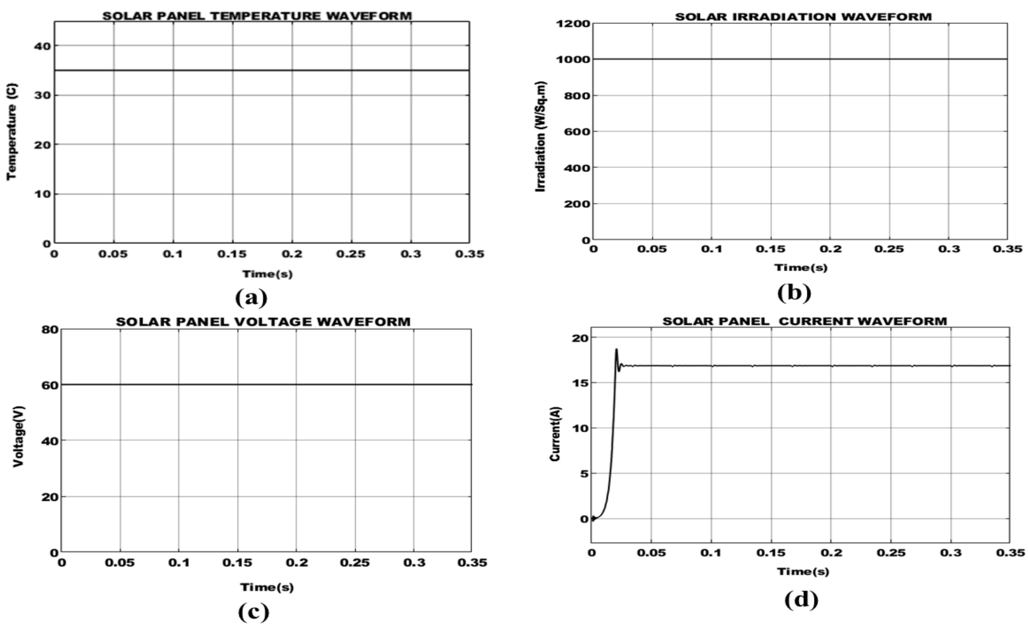


**Figure 9:** PV system parameters under constant working conditions

INTERNATIONAL JOURNAL OF PROGRESSIVE RESEARCH IN ENGINEERING MANAGEMENT AND SCIENCE (IJPREMS)
(Int Peer Reviewed Journal)
Vol. 04, Issue 10, October 2024, pp : 618-633
www.ijprems.com
editor@ijprems.com
e-ISSN : 2583-1062
Impact Factor : 7.001

Initially, the working of the KSK converter is tested by keeping both the ambient temperature and irradiance at a constant value. This test is mainly carried out to evaluate the working of KSK converter in standardized or ideal conditions and establish a benchmark performance. On observing the waveforms provided in Figure 9, it is evident that under ideal conditions with a fixed temperature and constant irradiance level, the PV system output remains stable without exhibiting any variations in voltage or current.

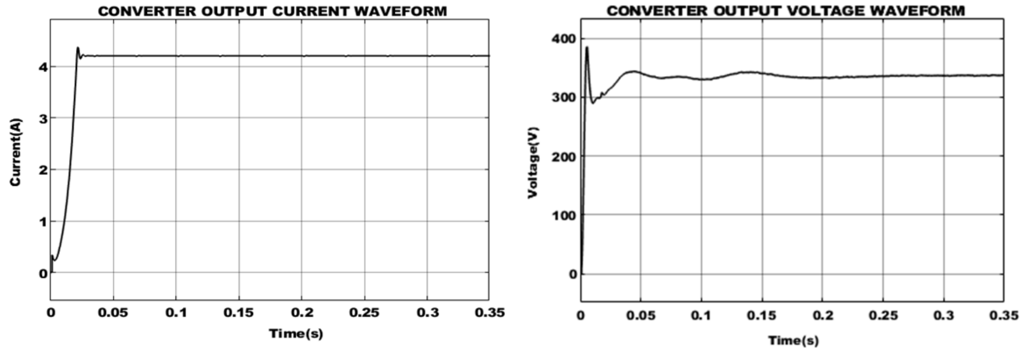


(a) (b)

**Figure 10:** KSK converter waveforms for constant working conditions (a) Output current and (b) Output voltage

As seen in the waveforms provided in Figure 10, when the stable voltage and current is provided as input to the KSK, the obtained output voltage and current waveforms are also stable. Here, the voltage is increased from 60V to 380V, while the current varies from 17A to 4.2A. Moreover, the voltage waveform is also seen to take 0.2s to attain a stable value. This stabilization time represents the transient response of the converter to adjust to the new operating conditions and reach a steady-state operation.

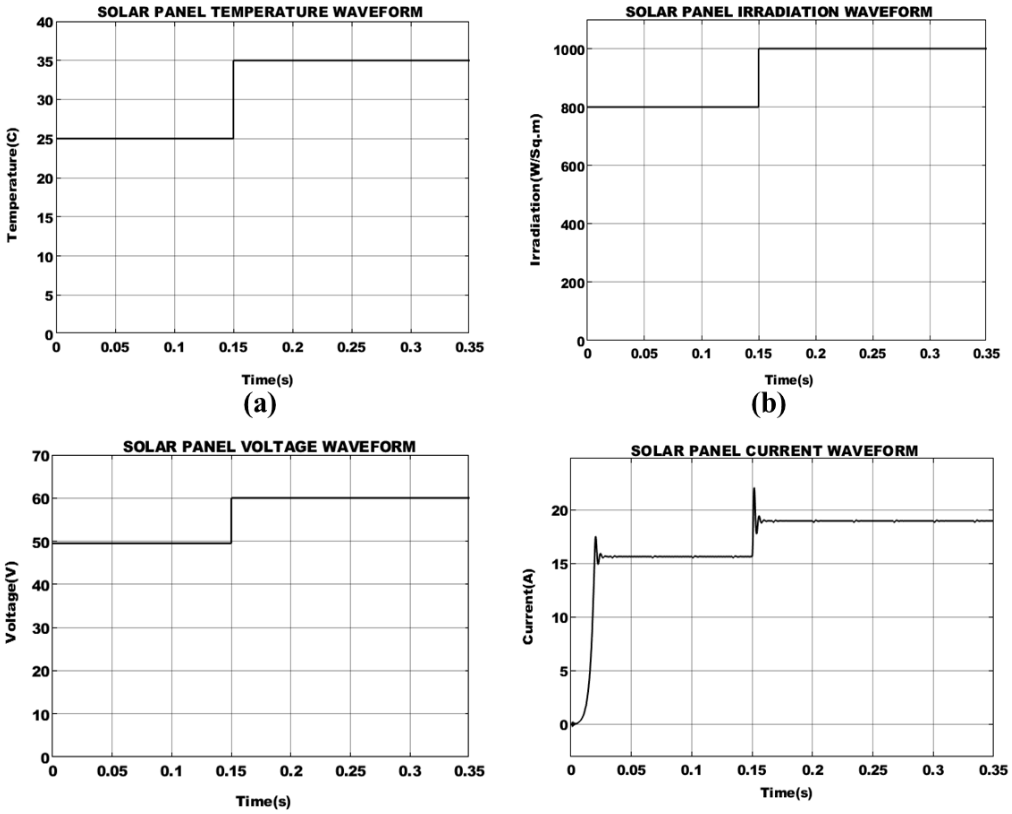


(c) (d)

**Figure 11:** PV system parameters under dynamic working conditions

In real-world scenarios, temperature and irradiance are rarely constant as they vary throughout the day due to weather changes, cloud cover, shading effects, and other environmental factors. Hence, to accurately simulate the performance of KSK converter in PV application, it is vital to consider and incorporate these variable operating conditions into the simulation. Hence, at 0.15s, an abrupt increase is introduced in both temperature and irradiance as seen in Figure 11 to allow for a more accurate representation of real-world scenarios. The immediate effect of these changes is clearly evident on the output voltage and current waveforms of the PV system, as they also undergo a sharp increase at 0.15s.

INTERNATIONAL JOURNAL OF PROGRESSIVE RESEARCH IN ENGINEERING MANAGEMENT AND SCIENCE (IJPREMS)
(Int Peer Reviewed Journal)
Vol. 04, Issue 10, October 2024, pp : 618-633
www.ijprems.com
editor@ijprems.com
e-ISSN : 2583-1062
Impact Factor : 7.001

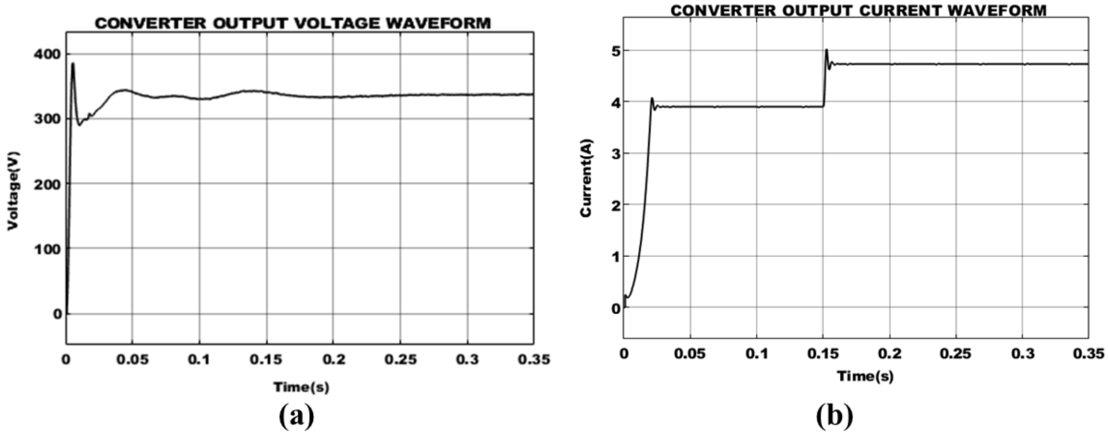


**Figure 12:** KSK converter waveforms for dynamic working conditions (a) Output current and (b) Output voltage

The KSK converter just takes 0.2s to attain a stable output voltage level as seen from the waveform given in Figure 12(a). The presence of ripples in the KSK converter output is also noted to be a bare minimum, which in turn assures a smooth and reliable power output from the converter. Moreover, the role of RBFNN MPPT in achieving the improved stability and reduced ripples in the output waveform of the KSK converter cannot be understated. Since, the real-time control signals provided by the RBFNN MPPT have effectively aided the KSK converter to mitigate the impact of variations in operating conditions. Likewise, the quick settling time of the KSK converter ascertains for its faster response to input condition changes and improved dynamic performance.

**Hardware Analysis**

The hardware analysis of the proposed approach is executed by developing a 1kW lab-scaled prototype of KSK converter as seen in Figure 13 using FPGA Spartan 6E controller. Here, the power supply for the laboratory setup is derived from a 15V power supply. The KSK converter in the form of a compact circuit is designed on a Printed Circuit Board (PCB). The interleaved switches of the converter circuit provide the much-needed ripple current reduction property, resulting in enhanced efficiency. The FPGA Spartan 6E controller in addition to controlling the switches of KSK converter, also supports the RBFNN MPPT implementation. The programmability of the FPGA Spartan 6E microcontroller allows for flexibility in implementing and optimizing the control algorithms, and the RBFNN MPPT enhances the tracking accuracy of the MPP, resulting in improved energy harvesting efficiency. Moreover, the driver circuit is responsible for providing the necessary gate drive signals to control the switching operation of the KSK converter power switches. It interfaces between the FPGA microcontroller and the power switches, ensuring accurate and timely control of the converter operation. The role of Digital Storage Oscilloscope (DSO) is to allow for the accurate and detailed observation of the KSK converter input and output waveforms. It aids in troubleshooting, performance optimization, and system validation. Furthermore, the developed hardware setup is also tested under both


**Figure 13:** 1kW lab-scaled prototype of PV fed DC-DC KSK converter with RBFNN MPPT

INTERNATIONAL JOURNAL OF PROGRESSIVE RESEARCH IN ENGINEERING MANAGEMENT AND SCIENCE (IJPREMS)
(Int Peer Reviewed Journal)
Vol. 04, Issue 10, October 2024, pp : 618-633
www.ijprems.com
editor@ijprems.com
e-ISSN : 2583-1062
Impact Factor : 7.001

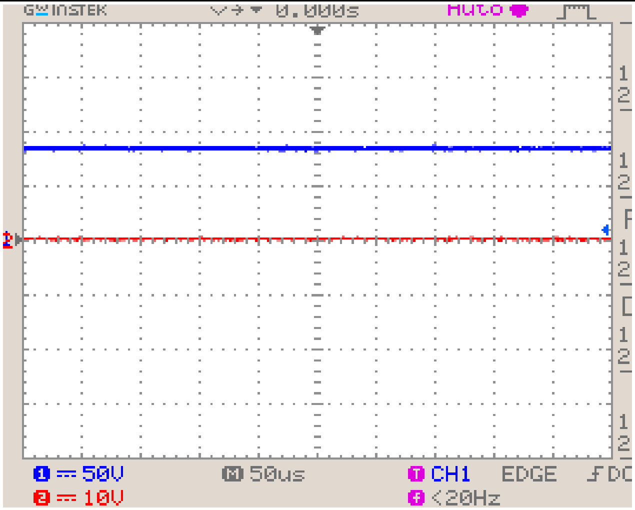


**Figure 14:** PV panel voltage under ideal working scenario

The hardware setup is tested under ideal working scenario, which refers to the constant temperature and irradiance conditions. This allows the establishment of a baseline performance measurement by supporting the evaluation of converter efficiency, stability and power output when the environmental variables are fixed. The waveform given in Figure 14 represents the PV output voltage in ideal working scenario. Here, under constant temperature and irradiance conditions, the PV system operates in a steady-state condition, which in turn leads to the relatively constant output voltage waveform. Moreover, the RBFNN MPPT ensures that the KSK converter operates at the MPP of the PV array.

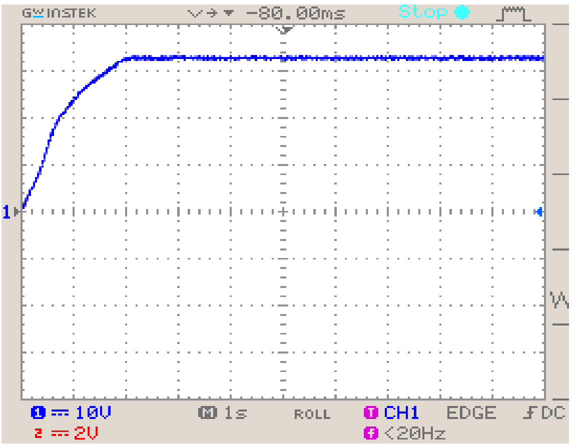


**Figure 15:** KSK converter output voltage under ideal working scenario

Under ideal working scenario, the output voltage from the KSK converter is also noted to be stable and constant as seen in Figure 15. Moreover, with the support of the RBFNN MPPT, the KSK converter takes less time to deliver a constant voltage output. Once the settling time has elapsed, the output voltage and current of the KSK converter stabilize at their desired values. The stable output ensures that the KSK converter delivers the required power to the load consistently, meeting the load's demands and maintaining a reliable power supply.

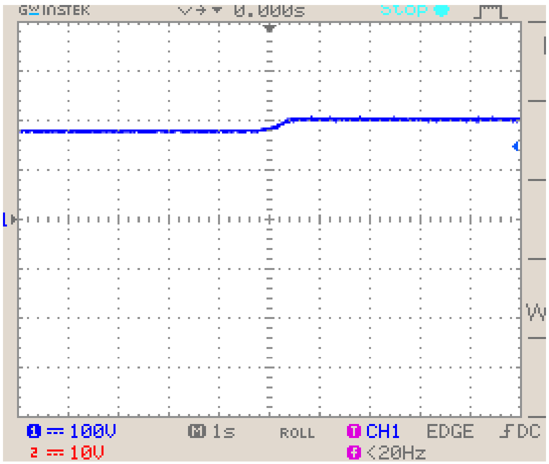


**Figure 16:** PV panel voltage under dynamic working scenario

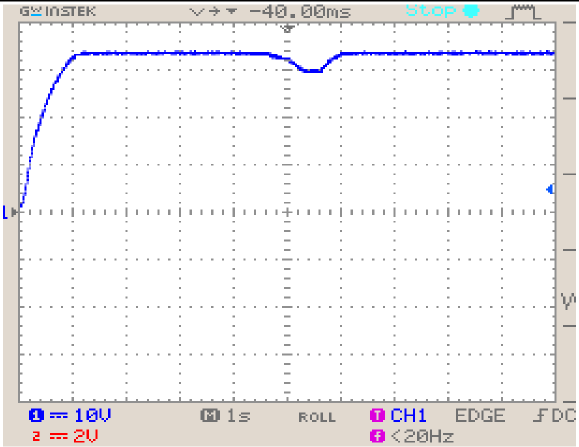


**Figure 17:** KSK converter voltage under dynamic working scenario

Executing the laboratory setup in a dynamic working scenario is essential to evaluate the performance and robustness of the system under real-world conditions where temperature and irradiance vary. By subjecting the setup to dynamic scenarios, the ability of the KSK converter to adapt to changing environmental conditions and maintain stable operation is assessed. The output voltage waveform of the PV system under dynamic condition as seen in Figure 16 is not constant. The impact of this variable input voltage is however, very low in the output voltage waveform of the KSK converter, which is provided in Figure 17. Here, the converter voltage recovers immediately from the momentary dip to deliver the desired stable voltage level. Hence, it is seen that the KSK converter along with RBFNN MPPT are capable of handling both ideal and dynamic working scenarios.

**Real Time Monitoring Using IoT**

The PV system is monitored real time using IoT and the parameters that are measured are displayed in the webpage as seen in Figure 18. Here, the real time monitoring of ambient temperature, irradiance, $V_{PV}$ *and* $I_{PV}$ is accomplished with the aid of sensors that collect information about every incessant changes in these parameters. The Node MCU collects data from the sensors, establishes a connection with the MySQL database in the cloud, and sends the data for storage.

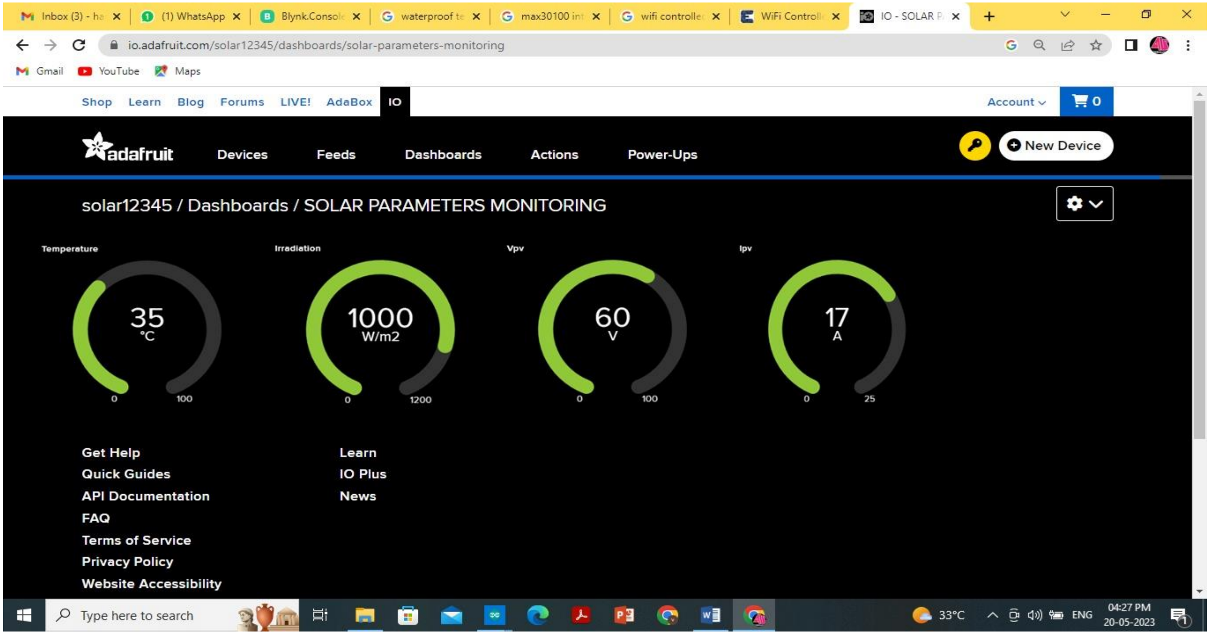


**Figure 18:** IoT webpage that monitors solar parameters

The web application retrieves the stored data from the database and displays it on the webpage, allowing users to monitor the PV system's performance in real-time. Here, the web application is created to retrieve the data from the database and present it in a user-friendly format. This allows users to remotely monitor and analyse the PV system's performance, including variables such as temperature, irradiance, PV voltage, and PV current.

**Comparative Analysis with Existing technologies**

The characteristics of the proposed KSK converter is studied against several other recently published converter topologies and the obtained results are given in Table 3. The converters considered are all high gain converters and they are evaluated in terms of component count, component voltage stress, efficiency and voltage gain.

INTERNATIONAL JOURNAL OF PROGRESSIVE RESEARCH IN ENGINEERING MANAGEMENT AND SCIENCE (IJPREMS)
(Int Peer Reviewed Journal)
Vol. 04, Issue 10, October 2024, pp : 618-633
www.ijprems.com
editor@ijprems.com
e-ISSN : 2583-1062
Impact Factor : 7.001

**Table 3:** Comparative analysis of several published converter

| Ref | T/C/D/I/S | Voltage gain | Published Year | Voltage stress on S | Voltage stress on D | Efficiency |
|---|---|---|---|---|---|---|
| [2] | 10/3/3/2/2 | $\frac{3+D}{3-D}$ | 2023 | $\frac{1}{3+D}$ | $\frac{2}{3+D}$ | 92.5% |
| [4] | 14/5/2/4/2 | $\frac{2D(2-D)}{(1-D)^2}$ | 2021 | $\frac{1}{(1-D)^2}$ | $\frac{2-D}{(1-D)^2}$ | 87.5% |
| [5] | 10/3/3/2/2 | $\frac{1-D+D^2}{(1-D)^2}$ | 2020 | $\frac{3D-2}{(1-D)^2}$ | $\frac{2D-1}{(1-D)^2}$ | - |
| [6] | 10/3/3/2/2 | $\frac{1+D}{(1-D)^2}$ | 2021 | $\frac{1+D}{(1-D)^2}$ | $\frac{2}{(1-D)^2}$ | 92% |
| [7] | 10/3/3/2/2 | $\frac{D^2}{(1-D)^2}$ | 2021 | $\frac{1}{(1-D)^2}$ | $\frac{D}{(1-D)^2}$ | 88.43% |
| [11] | 16/6/6/3/1 | $\frac{3-D}{(1-D)^2}$ | 2021 | $\frac{D}{(1-D)^2}$ | $\frac{1}{(1-D)^2}$ | 97.80% |
| [20] | 14/5/6/2/1 | $\frac{2(2-D)}{(1-D)^2}$ | 2021 | $\frac{D}{(1-D)^2}$ | $\frac{2-D}{(1-D)^2}$ | 95% |
| [21] | 12/4/3/3/2 | $\frac{D(1+D)}{(1-D)^2}$ | 2019 | $\frac{D}{(1-D)^2}$ | $\frac{D}{(1-D)^2}$ | 94.9% |
| [9] | 15/6/4/4/1 | $\frac{(1+D)(N+D)}{(1-D)^2}$ | 2019 | - | - | 90% |
| Proposed | 11/3/3/3/2 | $\frac{2-D}{1-D}$ | - | $\frac{1}{2-D}$ | $\frac{1}{2-D}$ | 98.6% |

$T - Total, C - Capacitor, D - Diode, I - Inductor, S - switch, N - Turns\ ratio$

The converters introduced in [7], [21] and [5] has the drawback of minimum voltage gain profile. Similarly, the converters introduced in [2] and [6] have a higher voltage stress profile, which results in potential reliability issues. The converter design in [21] in spite of offering several unique advantages, is confronted with the limitation in efficiency at extreme duty cycle. This limitation is however, highly critical in applications with varying duty cycle. In case of converters in [7], [4], [20] and [11], the problems like higher output voltage ripple and limited power handling ability are widely persistent. On analysing Table 3, it is apparent that KSK converter irrespective of its interleaved architecture has a fairly minimum component count. Moreover, it is also effective in outshining the other converter topologies with a peak efficiency value of 98.6%. Likewise, the voltage stress profile of KSK converter is also lesser than the other converters. According to information provided in Table 4, the KSK converter is also effective in outperforming the other interleaved converter topologies in terms of its high efficiency. From Figure 19, it is seen that the KSK converter has the highest voltage gain, which in turn allows it to have better compatibility with different energy sources, minimum current stress and wide input voltage range.

**Table 4:** Comparative analysis of several published Interleaved converter

| Ref | Converter | T/C/D/I/S | Published Year | Voltage gain | Efficiency |
|---|---|---|---|---|---|
| [12] | Interleaved SEPIC | 11/3/2/4/2 | 2021 | $\frac{D}{1-D}$ | 98% |
| [13] | Interleaved Boost | 8/1/2/3/2 | 2019 | $\frac{2D(2-D)}{(1-D)^2}$ | 96% |
| [14] | Interleaved Luo | 11/3/4/2/2 | 2020 | $3\left(\frac{2-D}{1-D}\right)$ | 97% |
| [22] | Interleaved Buck-Boost | 7/1/0/2/4 | 2022 | $\frac{D}{1-D}$ | 95.6% |

| | | | | | |
|---|---|---|---|---|---|
| [23] | Interleaved Boost-Cuk | 14/4/4/4/2 | 2022 | $\frac{3+D+2N}{1-D}$ | 88.43% |
| [24] | Interleaved Boost-SEPIC | 11/4/0/3/4 | 2019 | $\frac{D}{1-D}$ | 96.1% |
| Proposed | KSK converter | 11/3/3/3/2 | - | $\frac{2-D}{1-D}$ | 98.6% |

**Table 5:** Comparison of MPPT

| Ref | MPPT | Performance in varying conditions | Dynamic response | Sensed Parameters | Efficiency |
|---|---|---|---|---|---|
| [25] | P&O with Buck converter | Average | Varies | $V_{PV}, I_{PV}$ | 95.3% |
| [25] | IC with Buck converter | Average | Varies | $V_{PV}, I_{PV}$ | 95.4% |
| [25] | FOCV with Buck converter | Average | Medium | $V_{PV}, I_{PV}$ | 93.5% |
| [18] | ANN with Boost converter | Good | Fast | $V_{PV}, I_{PV}$ | 99.35% |
| [18] | FLC with Boost converter | Good | Fast | $V_{PV}, I_{PV}$ | 96.57% |
| [18] | ANN-FLC with Boost converter | Good | Fast | $V_{PV}, I_{PV}$ | 99.81% |
| Proposed | RBFNN with KSK converter | Excellent | Very Fast | $V_{PV}, I_{PV}$ | 99.89% |

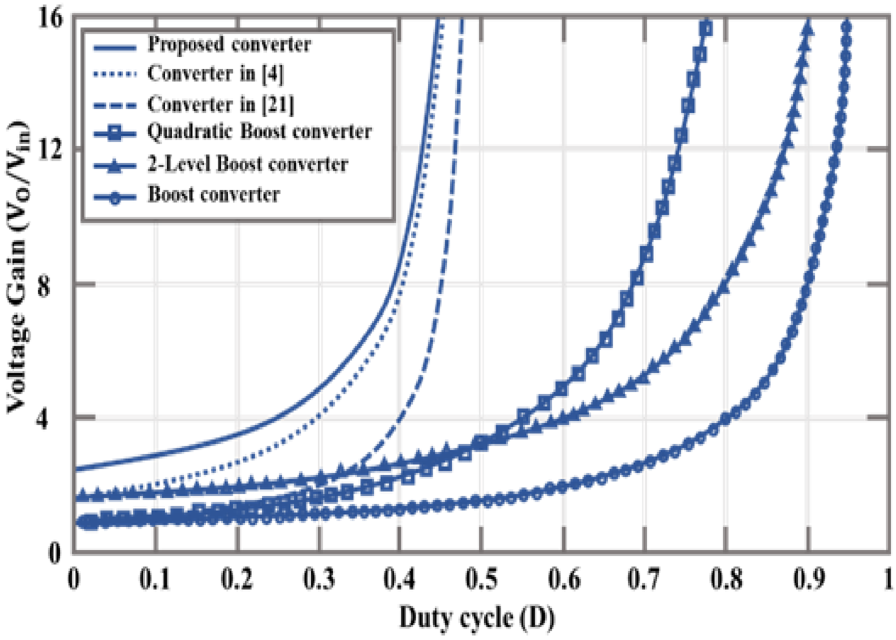


**Figure 19:** Comparison of converter voltage gain deviation against duty cycle

From Table 5, it is seen that the RBFNN MPPT performs better than other prominently used MPPT techniques as it operates with 99.89%. Moreover, it gives an excellent performance in varying operating conditions with quick dynamic response. Thus, it is apparent that the RBFNN MPPT provides a powerful and adaptive modelling capability that accurately estimates the MPP even under changing environmental conditions. The RBFNN MPPT algorithms mitigates oscillations around the MPP and reduce steady-state error. Furthermore, the adaptive learning capability of the RBFNN allows it to continuously update its model based on real-time measurements, leading to smoother and more stable tracking of the MPP.

INTERNATIONAL JOURNAL OF PROGRESSIVE RESEARCH IN ENGINEERING MANAGEMENT AND SCIENCE (IJPREMS)
(Int Peer Reviewed Journal)
Vol. 04, Issue 10, October 2024, pp : 618-633
www.ijprems.com
editor@ijprems.com
e-ISSN : 2583-1062
Impact Factor : 7.001

## 5. CONCLUSION

A novel KSK converter, which is an enhanced and efficient power conversion solution to PV system is introduced in this work. Aside from PV systems, the KSK converter is also compatible with other RESs due to its high voltage gain. Moreover, its features of high efficiency, better voltage regulation, and versatility make it suitable for many power conversion requirements in different industries. The tangible proof for the superior performance of the suggested KSK converter is obtained by undertaking both simulation and lab-scaled prototype implementation. These evaluation techniques are executed in both ideal and dynamic working scenarios with KSK converter displaying extraordinary performance in every operating conditions. The KSK converter is also triumphant over other recently published high gain converter topologies with minimum voltage stress profile, higher voltage gain profile and excellent conversion efficiency. Additionally, it is also clear that the RBFNN MPPT transcends the predicaments faced by conventional topologies by ensuring accurate MPP tracking even in dynamic operating conditions. Moreover, the proposed KSK converter also excels over other interleaved converter topologies with its strikingly high efficiency of 98.6%.

## 6. REFERENCES

[1] Qazi, Atika, Fayaz Hussain, Nasrudin ABD Rahim, Glenn Hardaker, Daniyal Alghazzawi, Khaled Shaban, and Khalid Haruna. "Towards sustainable energy: a systematic review of renewable energy sources, technologies, and public opinions." IEEE access 7 (2019): 63837-63851.

[2] Shaw, Priyabrata, Marif Daula Siddique, Saad Mekhilef, and Atif Iqbal. "A new family of high gain boost DC-DC converters with reduced switch voltage stress for renewable energy sources." International Journal of Circuit Theory and Applications 51, no. 3 (2023): 1265-1285.

[3] Ang, Tze-Zhang, Mohamed Salem, Mohamad Kamarol, Himadry Shekhar Das, Mohammad Alhuyi Nazari, and Natarajan Prabaharan. "A comprehensive study of renewable energy sources: classifications, challenges and suggestions." Energy Strategy Reviews 43 (2022): 100939.

[4] Yari, Keyvan, Seyed Hamid Shahalami, and Hamed Mojallali. "A novel nonisolated buck–boost converter with continuous input current and semiquadratic voltage gain." IEEE Journal of Emerging and Selected Topics in Power Electronics 9, no. 5 (2021): 6124-6138.

[5] Veerachary, Mummadi, and Nikhil Kumar. "Analysis and design of quadratic following boost converter." IEEE Transactions on Industry Applications 56, no. 6 (2020): 6657-6673.

[6] Naresh, S. V. K., Sankar Peddapati, and Mamdouh L. Alghaythi. "Non-Isolated High Gain Quadratic Boost Converter Based on Inductor's Asymmetric Input Voltage." IEEE Access 9 (2021): 162108-162121.

[7] Veerachary, Mummadi, and Malay Ranjan Khuntia. "Design and analysis of two-switch-based enhanced gain buck–boost converters." IEEE Transactions on Industrial Electronics 69, no. 4 (2021): 3577-3587.

[8] Balachander, K., A. Amudha, M. Siva Ramkumar, G. Emayavaramban, S. Divyapriy, and P. Nagaveni. "Design and analysis of modified CUK converter for electric hybrid vehicle." Materials Today: Proceedings 45 (2021): 1691-1695.

[9] Navamani, J. Divya, A. Lavanya, and K. Vijayakumar. "Modified SEPIC converter with high boosting capability." Electronics Letters 55, no. 13 (2019): 759-761.

[10] Nathan, Kumaran, Saikat Ghosh, Yam Siwakoti, and Teng Long. "A new DC–DC converter for photovoltaic systems: coupled-inductors combined Cuk-SEPIC converter." IEEE Transactions on Energy Conversion 34, no. 1 (2018): 191-201.

[11] Rahimi, Tohid, Lei Ding, Hossein Gholizadeh, Reza Sharifi Shahrivar, and Rasoul Faraji. "An ultra high step-up DC–DC converter based on the boost, Luo, and voltage doubler structure: Mathematical expression, simulation, and experimental." IEEE Access 9 (2021): 132011-132024.

[12] Kavin, K. S., and P. Subha Karuvelam. "PV-based grid interactive PMBLDC electric vehicle with high gain interleaved DC-DC SEPIC Converter." IETE Journal of Research (2021): 1-15.

[13] Spiazzi, Giorgio. "Analysis and design of the soft-switched clamped-resonant interleaved boost converter." CPSS Transactions on Power Electronics and Applications 4, no. 4 (2019): 276-287.

[14] Jegha, A. Darcy Gnana, M. S. P. Subathra, Nallapaneni Manoj Kumar, and Aritra Ghosh. "Optimally tuned interleaved Luo converter for PV array fed BLDC motor driven centrifugal pumps using whale optimization algorithm—A resilient solution for powering agricultural loads." Electronics 9, no. 9 (2020): 1445.

[15] Abdel-Salam, Mazen, Mohamed Th El-Mohandes, and Mahmoud El-Ghazaly. "An efficient tracking of MPP in PV systems using a newly-formulated P&O-MPPT method under varying irradiation levels." Journal of Electrical Engineering & Technology 15 (2020): 501-513.

[16] Ibrahim, Mohammad Haziq, Swee Peng Ang, Muhammad Norfauzi Dani, Mohammad Ishlah Rahman, Rafidah Petra, and Sheik Mohammed Sulthan. "Optimizing Step-Size of Perturb & Observe and Incremental Conductance MPPT Techniques Using PSO for Grid-Tied PV System." IEEE Access 11 (2023): 13079-13090.

[17] Uprety, Sandip, and Hoi Lee. "A 0.65-mW-to-1-W photovoltaic energy harvester with irradiance-aware auto-configurable hybrid MPPT achieving> 95% MPPT efficiency and 2.9-ms FOCV transient time." IEEE Journal of Solid-State Circuits 56, no. 6 (2020): 1827-1836.

[18] Hichem, Louki, Omeiri Amar, and Merabet Leila. "Optimized ANN-fuzzy MPPT controller for a stand-alone PV system under fast-changing atmospheric conditions." *Bulletin of Electrical Engineering and Informatics* 12, no. 4 (2023): 1960-1981.

[19] Al-Majidi, Sadeq D., Maysam F. Abbod, and Hamed S. Al-Raweshidy. "Design of an intelligent MPPT based on ANN using a real photovoltaic system data." In 2019 54th International Universities Power Engineering Conference (UPEC), pp. 1-6. IEEE, 2019.

[20] Mahmood, Arshad, Mohammad Zaid, Javed Ahmad, Mohd Anas Khan, Shahrukh Khan, Zaid Sifat, Chang-Hua Lin, Adil Sarwar, Mohd Tariq, and Basem Alamri. "A non-inverting high gain DC-DC converter with continuous input current." IEEE Access 9 (2021): 54710-54721.

[21] García-Vite, Pedro Martín, Julio C. Rosas-Caro, Ana Lidia Martínez-Salazar, Jose de Jesus Chavez, Antonio Valderrábano-González, and Victor M. Sánchez-Huerta. "Quadratic buck–boost converter with reduced input current ripple and wide conversion range." IET Power Electronics 12, no. 15 (2019): 3977-3986.

[22] Babazadeh, Yaser, Mehran Sabahi, Ebrahim Babaei, and Sun Kai. "A New Continuous Input Current Nonisolated Bidirectional Interleaved Buck-Boost DC-DC Converter." International Transactions on Electrical Energy Systems 2022 (2022).

[23] Rong, Desheng, Xuanjin Sun, and Ning Wang. "A high step-up interleaved boost-Cuk converter with integrated magnetic coupled inductors." IET Renewable Power Generation 16, no. 3 (2022): 607-621.

[24] Prabhakaran, Prajof, and Vivek Agarwal. "Novel boost-SEPIC type interleaved DC–DC converter for mitigation of voltage imbalance in a low-voltage bipolar DC microgrid." IEEE Transactions on Industrial Electronics 67, no. 8 (2019): 6494-6504.

[25] Atri, Parag K., P. S. Modi, and Nikhil Shashikant Gujar. "Comparison of different MPPT control strategies for solar charge controller." In 2020 International Conference on Power Electronics & IoT Applications in Renewable Energy and its Control (PARC), pp. 65-69. IEEE, 2020.